Model-based image reconstruction of chemiluminescence using a plenoptic 2.0 camera

Hung Nien, Jeffrey A. Fessler, and Volker Sick

EECS Department and Mechanical Engineering Department
University of Michigan, Ann Arbor

ICIP 2015: Computational Imaging
Sept. 29, 2015

Disclosure

- Supported by NSF under grant number CBET–1402707
- Equipment support from Intel Corporation

Motivation: combustion in transparent engine cylinder

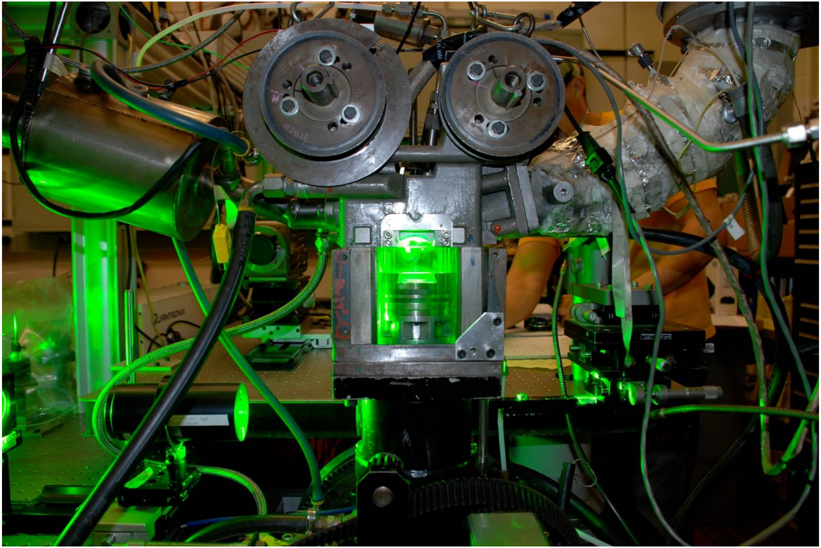

Motivation

Tomographic reconstruction of 3D chemiluminescence patterns such as flame fronts using a plenoptic camera.

Previous work

- Tomo-PIV (particle image velocimetry) (4–6 cameras) [Elsinga et al., 2006]
- Plenoptic 1.0 camera for PIV [Fahringer et al., 2012]
- Single-camera stereo [Greene et al., 2013] [Chen et al., 2015]

Depth maps for translucent objects?

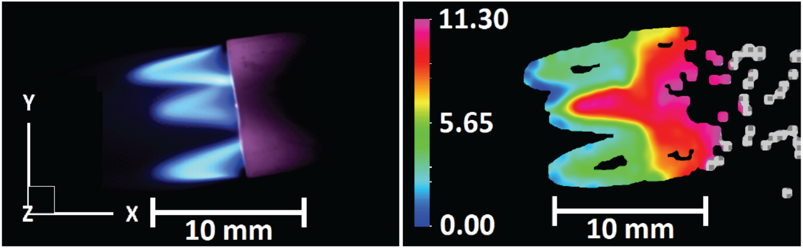

Plenoptic camera

Plenoptic cameras use micro-lens arrays to capture 4-D light field information of a scene. The angular information enables:

- depth estimation (for object surfaces illuminated externally) e.g., via triangulation [Perwaß, SPIE, 2012]
- tomographic reconstruction (for luminescent objects) (cf., digital X-ray tomosynthesis - limited-angle tomography).

◇ Images courtesy of Raytrix GmbH and Lytro, Inc.

Model-based image reconstruction (MBIR)

Overall goal: reconstruct 3D chemiluminescence pattern $\mathbf{x}$ from plenoptic camera measurement $\mathbf{y}$.

MBIR components:

- 3D object model (basis coefficients) $\mathbf{x}$
  - Image voxel, basis function, ...
- System model $\mathbf{A}$ ($\#$ of sensor elements $\times$ $\#$ of object voxels)
  - Linearity, finite voxel size, finite pixel size, ...
- Data noise statistics $\mathrm{p}(\mathbf{y}|\mathbf{Ax})$
  - Additive Gaussian, Poisson, ...
- Cost function $\Psi(\mathbf{x})$
  - Data fidelity, regularizer, physical constraints, ...
- Iterative algorithm ($\arg\min_{\mathbf{x}}$)
  - MART, FISTA, Newton's methods, ...

[Nuyts et al., Phys. Med. Biol., 2013]

Model-based image reconstruction (continued)

We reconstructed objects by solving a regularized LS problem:

$$\mathbf{x}^\star \in \arg\min_{\mathbf{x}} \left\{ \Psi(\mathbf{x}) \triangleq \frac{1}{2} \|\mathbf{y} - \mathbf{A}\mathbf{x}\|_2^2 + \mathsf{R}(\mathbf{x}) \right\} \text{ s.t. } \mathbf{x} \succeq \mathbf{0},$$

where R denotes an edge-preserving corner-rounded TV regularizer.

We focused on R defined as

$$\mathsf{R}(\mathbf{x}) \triangleq \sum_{i=1} \beta_i \sum_n \varphi_{\text{Huber}}([\mathbf{C}_i\mathbf{x}]_n),$$

- $\mathbf{C}_i$: finite difference matrix along ith direction
- β_i : corresponding regularization parameter.
- $\varphi_{\text{Huber}}(t) \approx |t|$

System model for a plenoptic camera

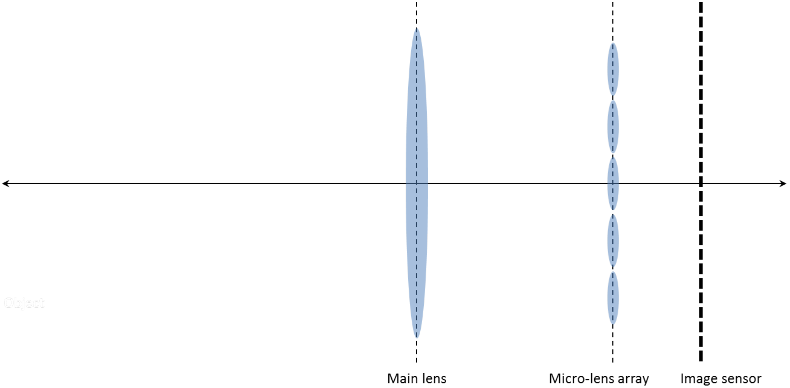

[Bishop & Favaro, IEEE T-PAMI, 2012]

System model for a plenoptic camera

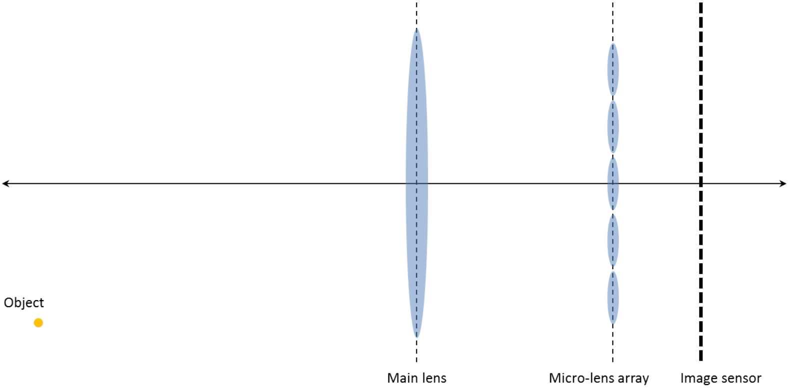

Build (pre-compute) system matrix **A** one column at a time

System model for a plenoptic camera

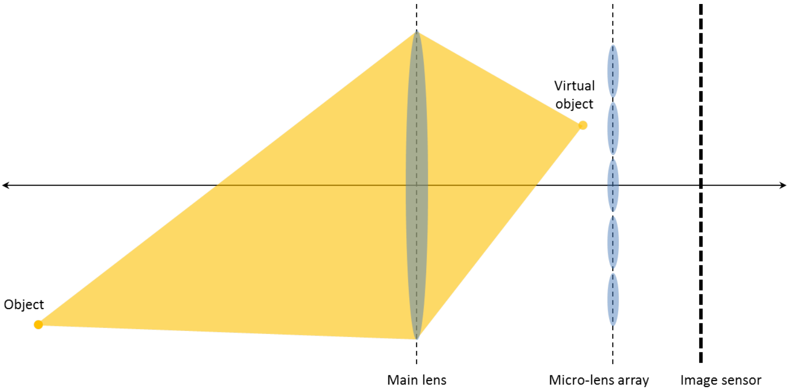

$$|\longleftarrow \quad z \quad \longrightarrow|\longleftarrow \quad Z \quad \longrightarrow|$$

thin lens formula: $1/z + 1/Z = 1/F$

System model for a plenoptic camera

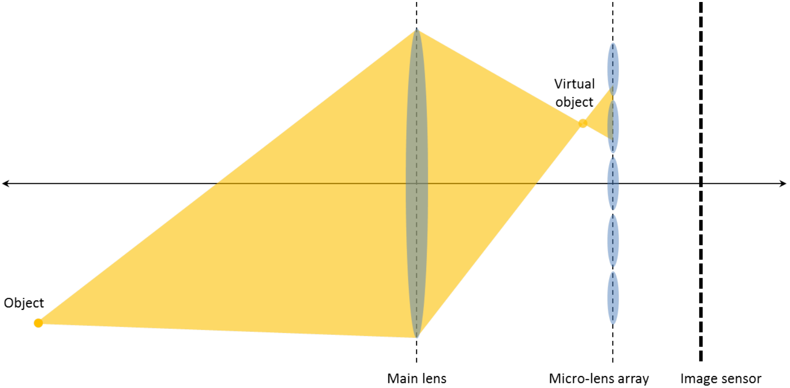

System model for a plenoptic camera

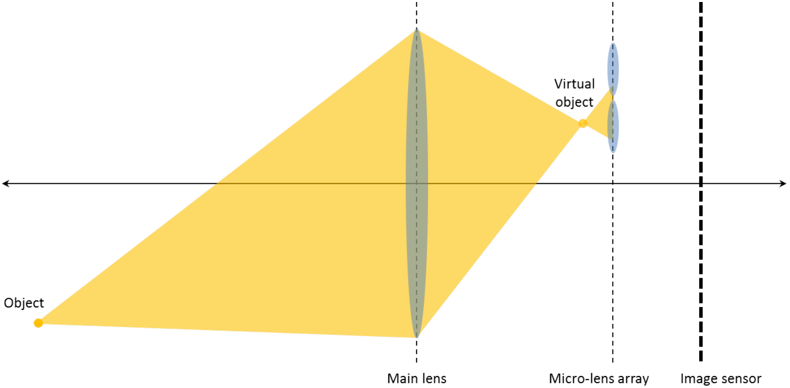

System model for a plenoptic camera

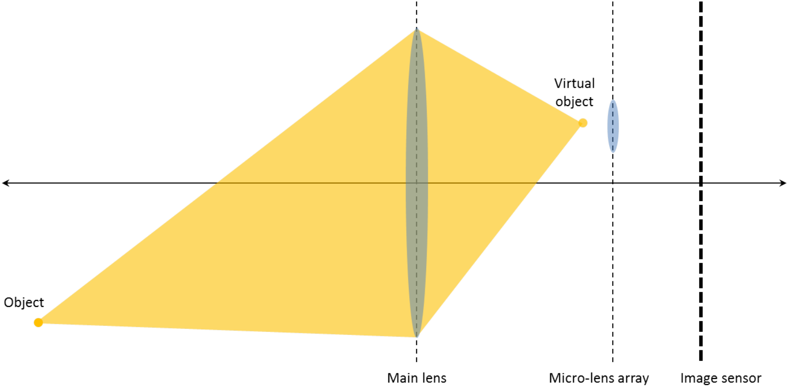

Use superposition to consider one microlens at a time

System model for a plenoptic camera

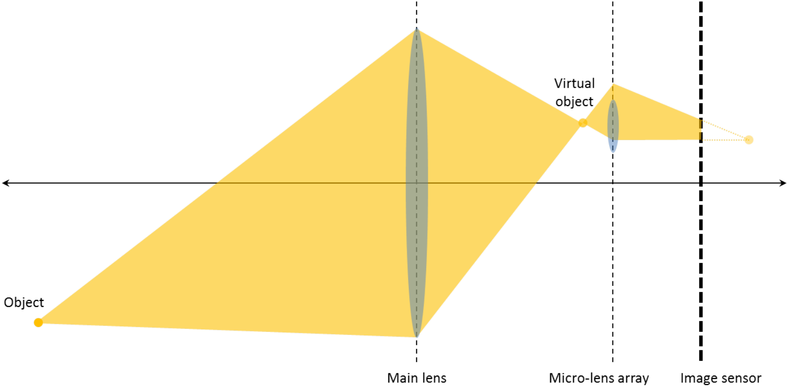

If microlens had large diameter...

System model for a plenoptic camera

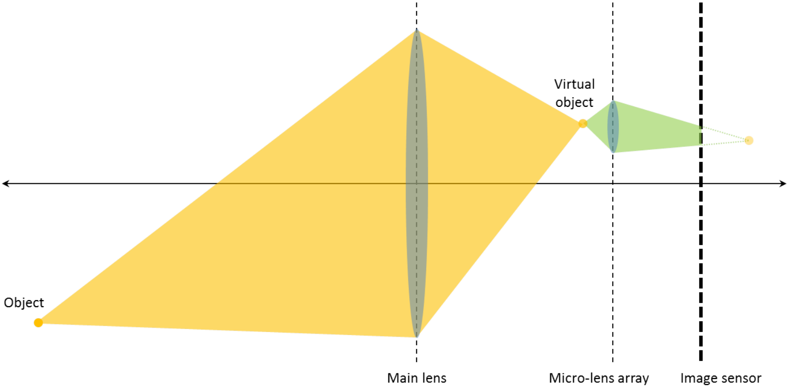

If main lens had large diameter...

System model for a plenoptic camera

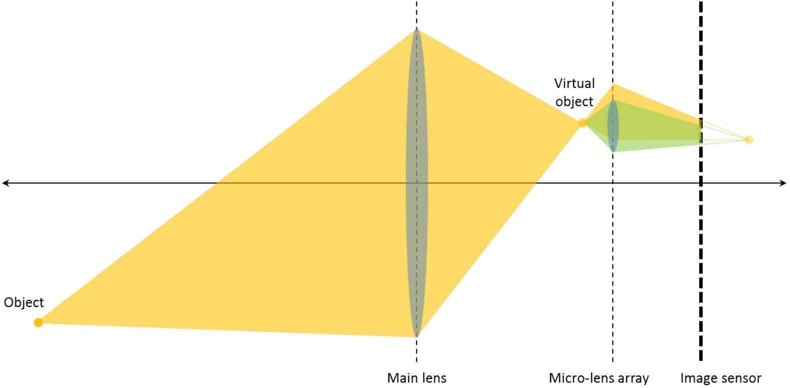

Combined effect of main lens and microlens

System model for a plenoptic camera

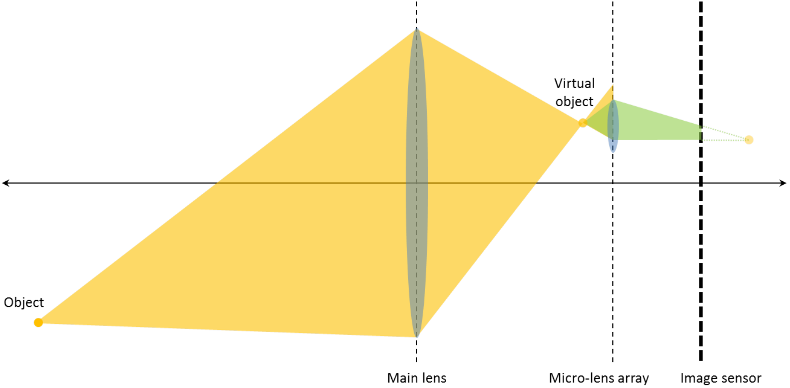

Combined effect of main lens and microlens

System model - continued

Continuous-space PSF of the *i*th micro-lens is:

$$\beta_i(s,t;x,y,z) = \underbrace{\beta_i^{\text{ML-}\mu\text{L}}(s,t;x,y,z)}_{\propto \operatorname{circ}\left(s,t;\mathbf{c}_i^{\text{ML-}\mu\text{L}},B_i\right)} \cdot \underbrace{\beta_i^{\mu\text{L}}(s,t;x,y,z)}_{\propto \operatorname{circ}\left(s,t;\mathbf{c}_i^{\mu\text{L}},b_i\right)},$$

where

- (s,t) denotes 2D sensor coordinates
- centers $\mathbf{c}_i^{\text{ML-}\mu\text{L}}$, $\mathbf{c}_i^{\mu\text{L}}$, and radii B_i, and b_i depend on the object point position (x,y,z) and camera geometry.
- $\sum_i \beta_i(s,t;x,y,z)$ sketched:

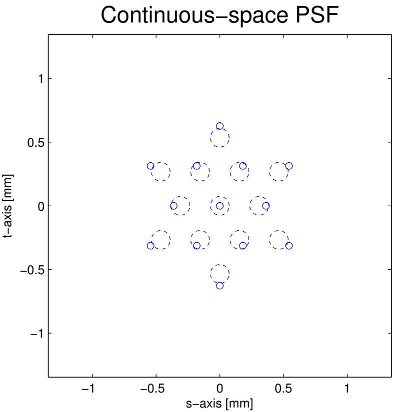

Computational challenges

- Dense micro-lens array
- Highly shift-variant point spread function
- Non-separable aperture / PSF (cf., X-ray CT)
- Lens aberrations
- Finite sensor pixel size
  The discrete PSF of a micro-lens consists of integrals of the circle-circle intersection over each sensor pixel, where the circle centers depend on the position of the "point source."

  We approximate each finite-sized sensor pixel as $L \times L$ infinitesimal pixels, i.e., $L\times$-subsampling in each direction.
- Finite object voxel size

Computational challenges

- Dense micro-lens array
- Highly shift-variant point spread function
- Non-separable aperture / PSF (cf., X-ray CT)
- Lens aberrations
- Finite sensor pixel size
  The discrete PSF of a micro-lens consists of integrals of the circle-circle intersection over each sensor pixel, where the circle centers depend on the position of the "point source."

  We approximate each finite-sized sensor pixel as $L \times L$ infinitesimal pixels, i.e., $L\times$-subsampling in each direction.
- Finite object voxel size

One (x, y) transaxial plane of a 3D object voxel

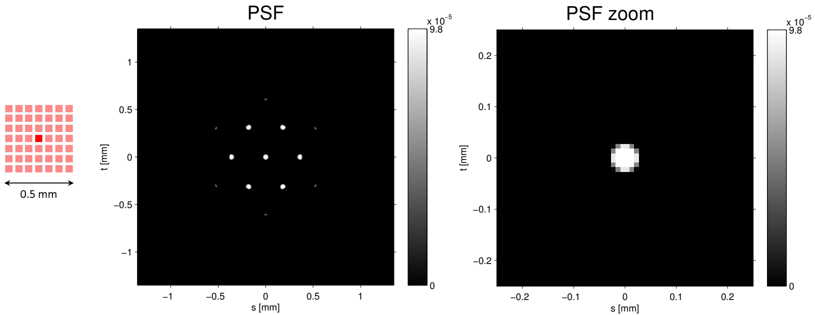

Finite-sized object voxel effects

One (x, y) transaxial plane of a 3D object voxel

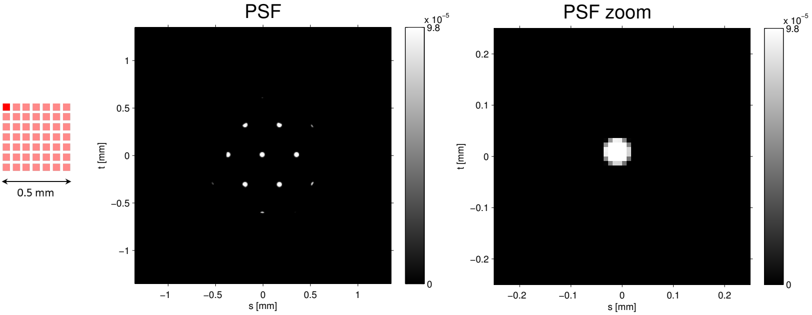

One (x, y) transaxial plane of a 3D object voxel

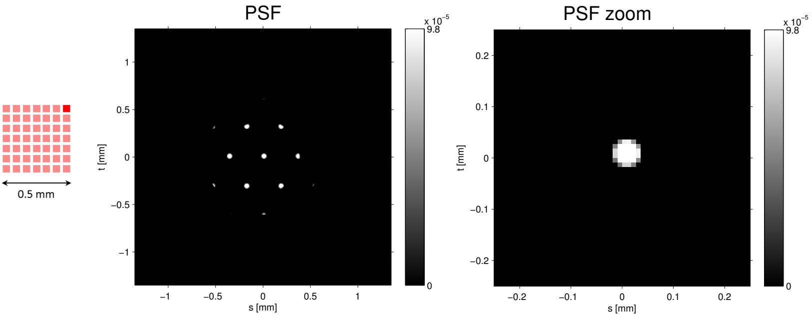

Finite-sized object voxel effects

One (x, y) transaxial plane of a 3D object voxel

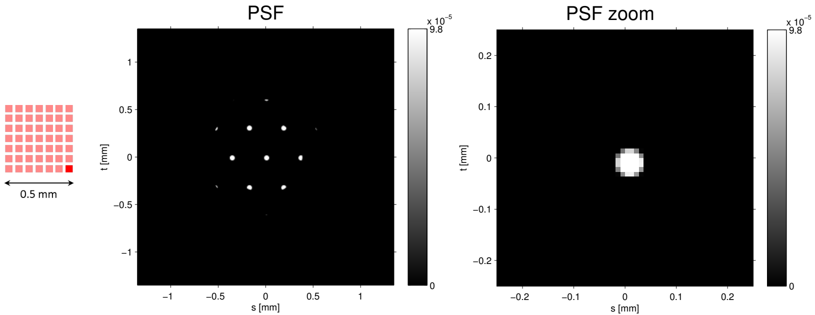

One (x, y) transaxial plane of a 3D object voxel

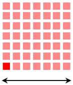

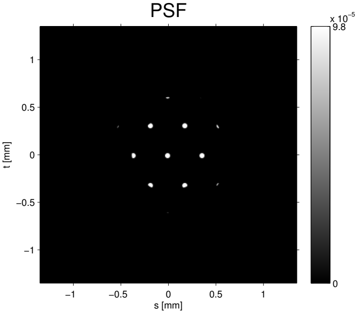

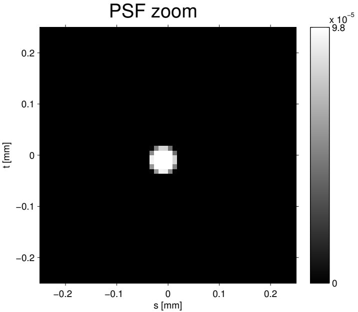

Finite-sized object voxel: baseline approximation

We approximate each cubic voxel as $K \times K \times K$ equally spaced infinitesimal voxels, i.e., $K\times$-subsampling in each direction.

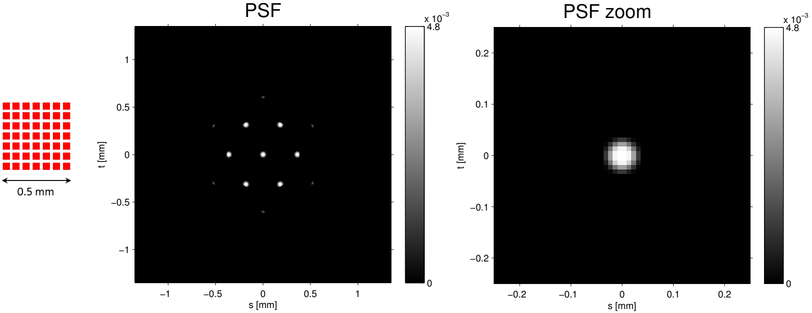

† We used $K = 7$ here.

Finite-sized object voxel: baseline approximation

We approximate each cubic voxel as $K \times K \times K$ equally spaced infinitesimal voxels, i.e., $K\times$-subsampling in each direction.

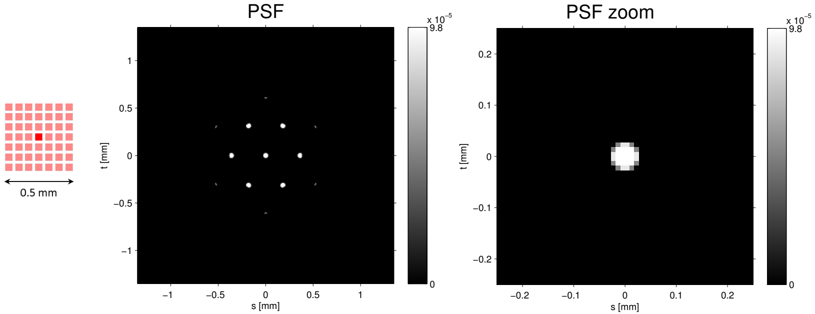

(infinitesimal)

Why finite voxel size matters

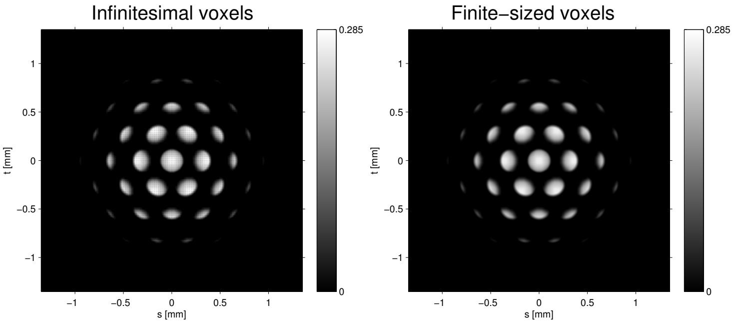

† Using $0.5 \times 0.5 \times 0.5$ [mm^3] cubic voxels and $K = 7$.

Why finite voxel size matters (zoomed)

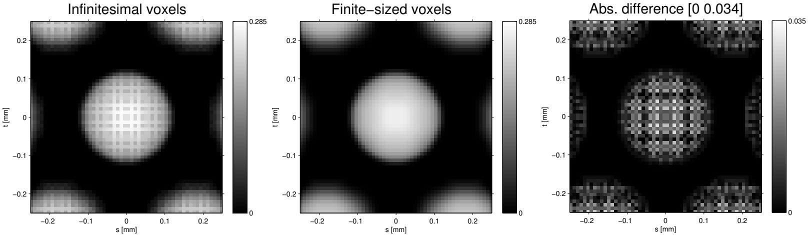

Numerical experiments: imaging geometry

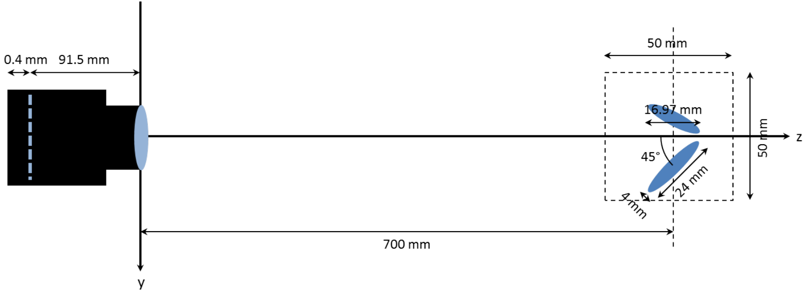

Numerical experiments: object geometry

- $100 \times 100 \times 100$ voxel object
- $0.5 \times 0.5 \times 0.5$ [mm^3] voxels
- 50 [mm] field-of-view
- $7\times$ sensor subsampling when precomputing $\mathbf{A}$
- 50 dB SNR (additive white Gaussian noise)

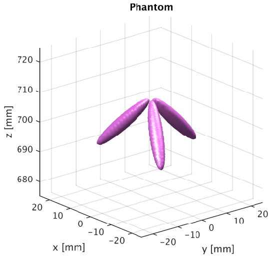

- To avoid an inverse crime when synthesizing plenoptic sensor pictures, we used a voxelized object having a $2\times$ finer grid in 3D, with $11\times$ subsampling per dimension.

Numerical experiments: object geometry

- $100 \times 100 \times 100$ voxel object
- $0.5 \times 0.5 \times 0.5$ [mm^3] voxels
- 50 [mm] field-of-view
- $7\times$ sensor subsampling when precomputing $\mathbf{A}$
- 50 dB SNR (additive white Gaussian noise)

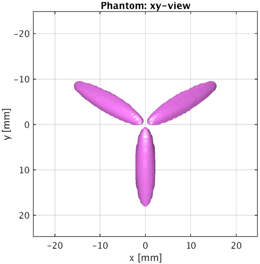

- To avoid an inverse crime when synthesizing plenoptic sensor pictures, we used a voxelized object having a $2\times$ finer grid in 3D, with $11\times$ subsampling per dimension.

Numerical experiments: object geometry

- $100 \times 100 \times 100$ voxel object
- $0.5 \times 0.5 \times 0.5$ [mm^3] voxels
- 50 [mm] field-of-view
- $7\times$ sensor subsampling when precomputing $\mathbf{A}$
- 50 dB SNR (additive white Gaussian noise)

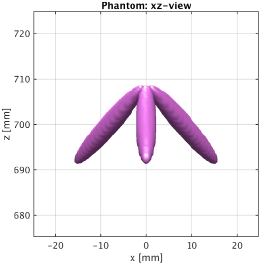

- To avoid an inverse crime when synthesizing plenoptic sensor pictures, we used a voxelized object having a $2\times$ finer grid in 3D, with $11\times$ subsampling per dimension.

Numerical experiments: plenoptic cameras

	Camera #1	Camera #2	Camera #3	
f_{main}	80	80	80	[mm]
f-number	1.4	2.8	1.4	
d_{main}	57.14	28.57	57.14	[mm]
f_{micro}	0.35	0.35	0.35	[mm]
d_{micro}	0.27	0.135	0.135	[mm]
type	larger	Bishop & Favaro	overlaps	

- 9μm $\times$ 9μm sensor pixel size
- 850×850 pixel sensor

Numerical experiments: plenoptic cameras

	Camera #1	Camera #2	Camera #3	
f_{main}	80	80	80	[mm]
f-number	1.4	2.8	1.4	
d_{main}	57.14	28.57	57.14	[mm]
f_{micro}	0.35	0.35	0.35	[mm]
d_{micro}	0.27	0.135	0.135	[mm]
type	larger	Bishop & Favaro	overlaps	

- 9µm $\times$ 9µm sensor pixel size
- 850 $\times$ 850 pixel sensor

Numerical experiments: plenoptic cameras

	Camera #1	Camera #2	Camera #3	
f_{main}	80	80	80	[mm]
f-number	1.4	2.8	1.4	
d_{main}	57.14	28.57	57.14	[mm]
f_{micro}	0.35	0.35	0.35	[mm]
d_{micro}	0.27	0.135	0.135	[mm]
type	larger	Bishop & Favaro	overlaps	

- 9µm $\times$ 9µm sensor pixel size
- 850 $\times$ 850 pixel sensor

Numerical experiments: simulated plenoptic pictures

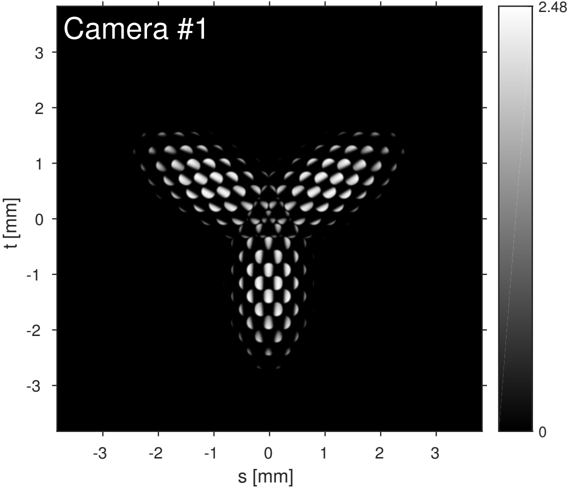

Better angular resolution than Camera #2, but worse spatial resolution

Numerical experiments: simulated plenoptic pictures

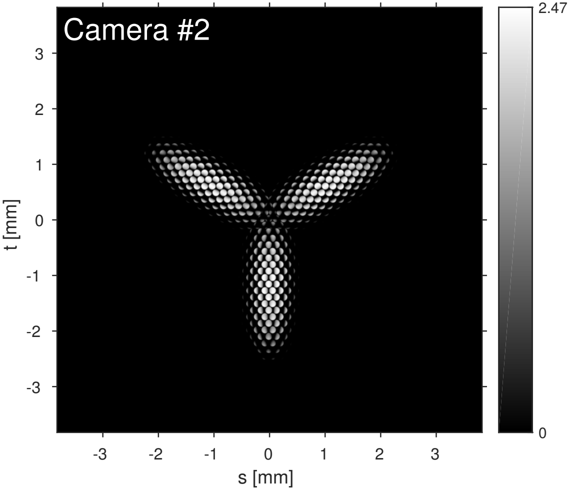

Bishop & Favaro, 2012

Numerical experiments: simulated plenoptic pictures

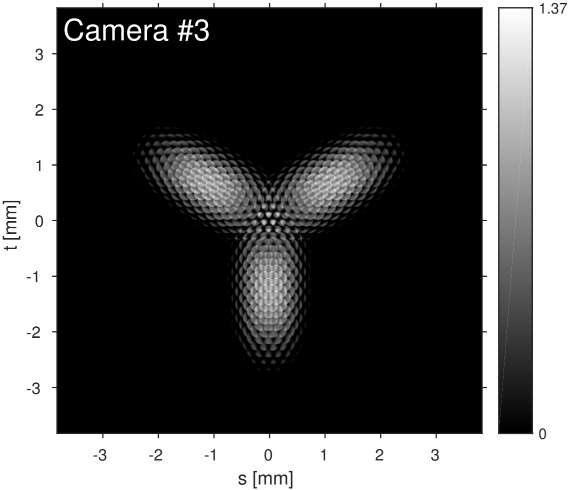

Overlapping (larger) subimages: demultiplexing needed, but (perhaps) more angular information than Camera #2.

Numerical experiments: image reconstruction

[Recap] Our image reconstruction problem is:

$$\mathbf{x}^\star \in \arg\min_{\mathbf{x}} \left\{ \Psi(\mathbf{x}) \triangleq \frac{1}{2} \|\mathbf{y} - \mathbf{A}\mathbf{x}\|_2^2 + \mathrm{R}(\mathbf{x}) \right\} \text{ s.t. } \mathbf{x} \succeq \mathbf{0}\,,$$

- 500 iterations of FISTA with adaptive restart
  [Beck & Teboulle, IEEE T-IP, 2009]
  [O'Donoghue & Candès, FCM, 2015]
- Precomputed / stored **A** (column-wise sparse)
  - $7\times$ object subsampling (x, y, z)
  - $7\times$ sensor subsampling (s, t)
  - 320 secs/slice for camera #1
    (60 threads @ MATLAB)
- 26 3D neighbors used in the (smoothed) TV regularizer

Numerical experiments: finite voxel size

Infinitesimal voxels

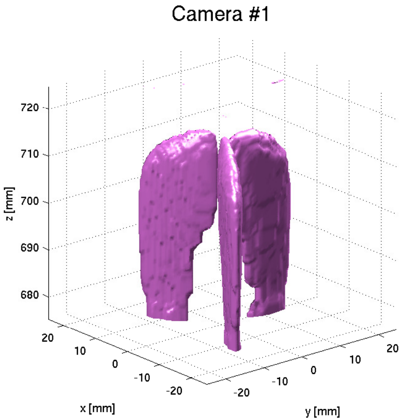

Finite-sized voxels

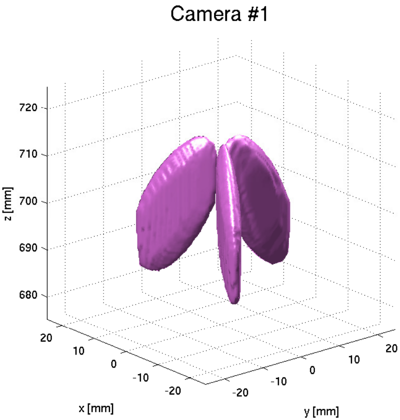

Contours at isovalue = 20% of maximum intensity.

Numerical experiments: aperture size

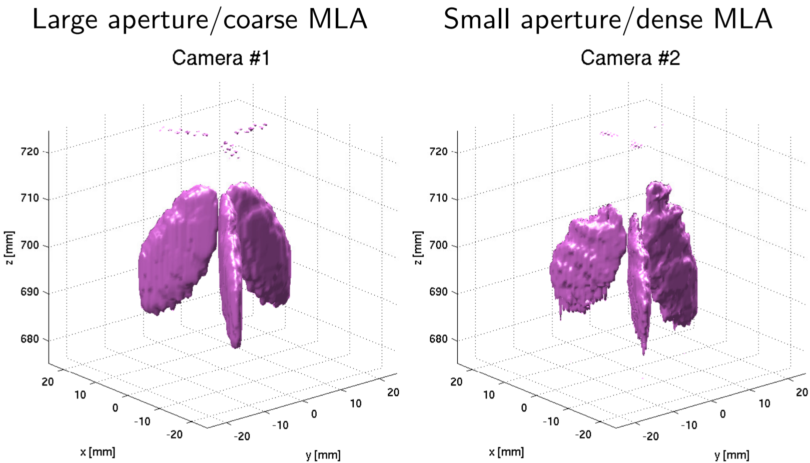

Better lateral resolution of Camera 2 not helpful here.

Numerical experiments: aperture size - slices

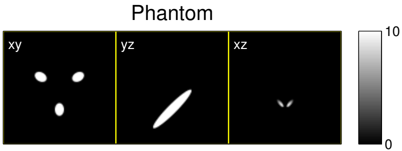

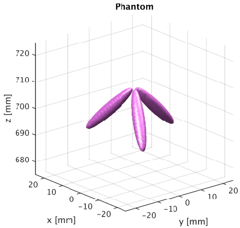

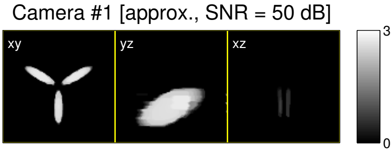

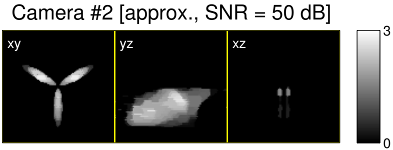

Numerical experiments: overlapping subimages

Non-overlapping subimages

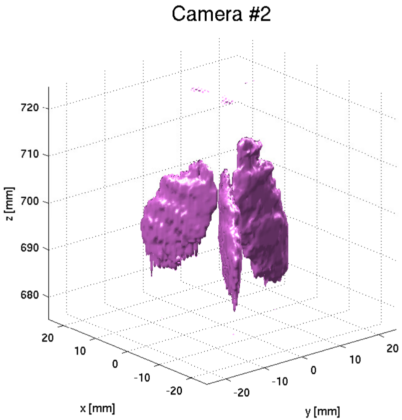

Overlapping subimages

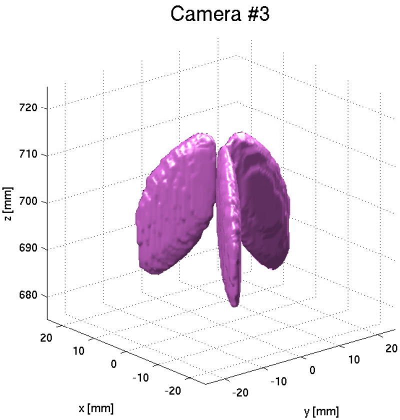

Numerical experiments: overlapping subimages - slices

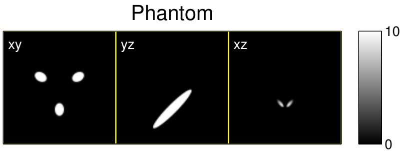

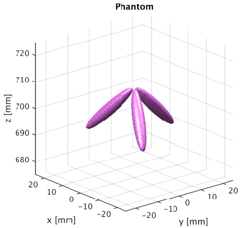

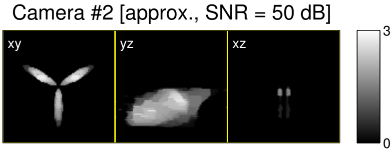

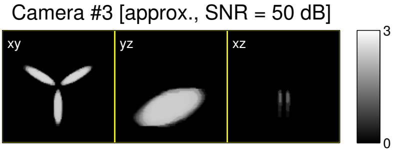

Numerical experiments: object distance

$d_{\text{object}} = 700$ [mm]

Camera #2

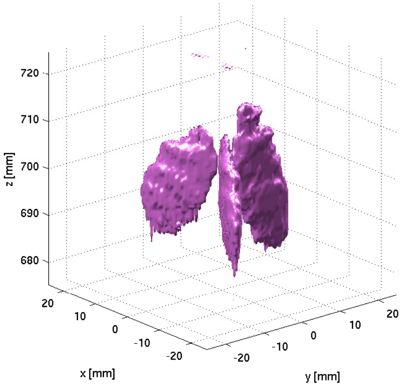

$d_{\text{object}} = 550$ [mm]

Camera #2

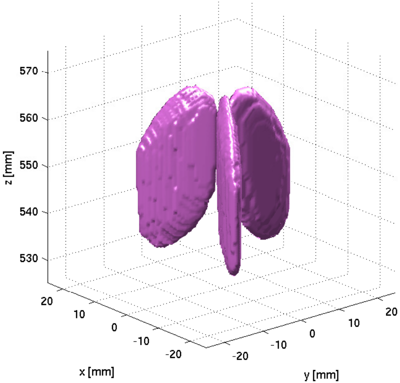

Numerical experiments: object distance - slices

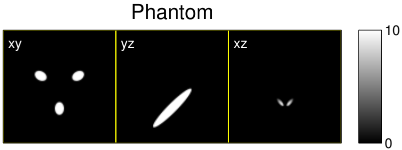

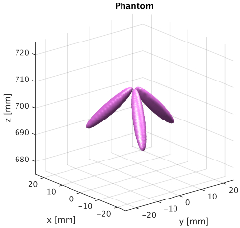

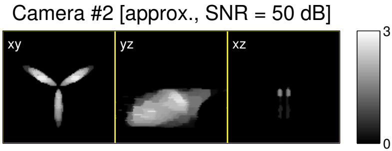

$d_{\text{object}} = 700$ [mm]

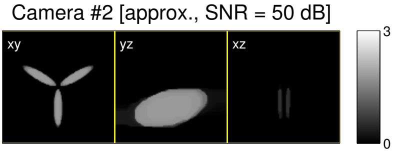

$d_{\text{object}} = 550$ [mm]

Numerical experiments: sharp vs smooth object

Sharp object edges

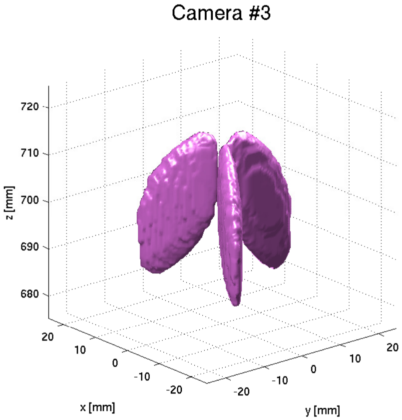

Smooth object edges

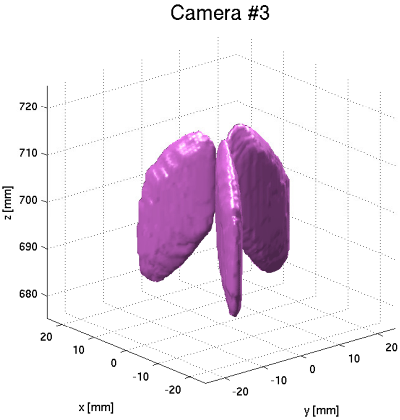

Numerical experiments: sharp vs smooth object - slices

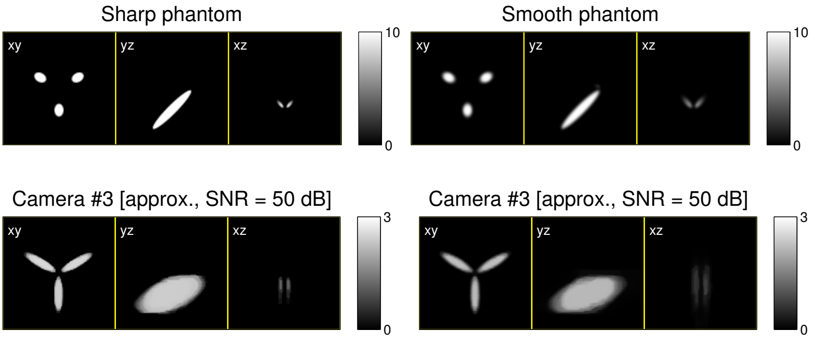

Conclusions

- Model-based image reconstruction may be viable for 3D chemiluminescence from plenoptic camera data
- Voxel-size modeling is important
- Larger angular range of incident light improves z-resolution (but more severe lens aberration?)
- F-number matching can be relaxed (overlapping sub-images) to improve depth resolution in tomographic formulation
- Need fast on-the-fly forward/back-projections to solve real large-scale image reconstruction problems

Conclusions

- Model-based image reconstruction may be viable for 3D chemiluminescence from plenoptic camera data
- Voxel-size modeling is important
- Larger angular range of incident light improves z-resolution (but more severe lens aberration?)
- F-number matching can be relaxed (overlapping sub-images) to improve depth resolution in tomographic formulation
- Need fast on-the-fly forward/back-projections to solve real large-scale image reconstruction problems

Conclusions

- Model-based image reconstruction may be viable for 3D chemiluminescence from plenoptic camera data
- Voxel-size modeling is important
- Larger angular range of incident light improves z-resolution (but more severe lens aberration?)
- F-number matching can be relaxed (overlapping sub-images) to improve depth resolution in tomographic formulation
- Need fast on-the-fly forward/back-projections to solve real large-scale image reconstruction problems

Conclusions

- Model-based image reconstruction may be viable for 3D chemiluminescence from plenoptic camera data
- Voxel-size modeling is important
- Larger angular range of incident light improves z-resolution (but more severe lens aberration?)
- F-number matching can be relaxed (overlapping sub-images) to improve depth resolution in tomographic formulation
- Need fast on-the-fly forward/back-projections to solve real large-scale image reconstruction problems

Conclusions

- Model-based image reconstruction may be viable for 3D chemiluminescence from plenoptic camera data
- Voxel-size modeling is important
- Larger angular range of incident light improves z-resolution (but more severe lens aberration?)
- F-number matching can be relaxed (overlapping sub-images) to improve depth resolution in tomographic formulation
- Need fast on-the-fly forward/back-projections to solve real large-scale image reconstruction problems

Bibliography

[1] G. E. Elsinga, B. Wieneke, F. Scarano, and A. Schröder, "Tomographic 3D-PIV and Applications," in *Particle Image Velocimetry*, Springer Berlin Heidelberg, 2008, pp. 103–25.

[2] T. W. Fahringer and B. S. Thurow, "Tomographic reconstruction of a 3-D flow field using a plenoptic camera," in *AIAA Fluid Dynamics Conf.*, 2012, p. 2826.

[3] M. L. Greene and V. Sick, "Volume-resolved flame chemiluminescence and laser-induced fluorescence imaging," *Appl Phys B*, vol. 113, no. 1, 87–92, Oct. 2013.

[4] H. Chen, P. Lillo, and V. Sick, "3D spray-flow interaction in a spark-ignition direct-injection engine," *Intl. J. Engine Research*, 2015, To appear.

[5] C. Perwass and L. Wietzke, "Single lens 3D-camera with extended depth-of-field," in *Proc. SPIE 8291 Human Vision and Electronic Imaging XVII*, 2012, p. 829 108.

[6] J. Nuyts, B. De Man, J. A. Fessler, W. Zbijewski, and F. J. Beekman, "Modelling the physics in iterative reconstruction for transmission computed tomography," *Phys. Med. Biol.*, vol. 58, no. 12, R63–96, Jun. 2013.

[7] T. E. Bishop and P. Favaro, "The light field camera: Extended depth of field, aliasing, and superresolution," *IEEE Trans. Patt. Anal. Mach. Int.*, vol. 34, no. 5, 972–86, May 2012.

[8] A. Beck and M. Teboulle, "Fast gradient-based algorithms for constrained total variation image denoising and deblurring problems," *IEEE Trans. Im. Proc.*, vol. 18, no. 11, 2419–34, Nov. 2009.

[9] B. O'Donoghue and E. Candès, "Adaptive restart for accelerated gradient schemes," *Found. Computational Math.*, vol. 15, no. 3, 715–32, Jun. 2015.

Approximate box blur

In practice, $B_i \gg b_i$, so β_i is usually a circle.
The continuous-space PSF of a voxel slice at depth z is

$$
\begin{aligned}
& \int_{x-\frac{\triangle_x}{2}}^{x+\frac{\triangle_x}{2}} \int_{y-\frac{\triangle_y}{2}}^{y+\frac{\triangle_y}{2}} \beta_i(s, t; \bar{x}, \bar{y}, z)\, d\bar{y}\, d\bar{x} \\
\approx & \int_{x-\frac{\triangle_x}{2}}^{x+\frac{\triangle_x}{2}} \int_{y-\frac{\triangle_y}{2}}^{y+\frac{\triangle_y}{2}} \operatorname{circ}\left(s, t; \mathbf{c}_i^{\mu\mathrm{L}}(\bar{x}, \bar{y}), b_i\right) d\bar{y}\, d\bar{x} \\
= & \int_{-\frac{\triangle_x}{2}}^{\frac{\triangle_x}{2}} \int_{-\frac{\triangle_y}{2}}^{\frac{\triangle_y}{2}} \operatorname{circ}\left(s, t; \mathbf{c}_i^{\mu\mathrm{L}}(x + \delta_x, y + \delta_y), b_i\right) d\delta_y\, d\delta_x \\
= & \iint \operatorname{circ}\left(s - \delta_s, t - \delta_t; \mathbf{c}_i^{\mu\mathrm{L}}(x, y), b_i\right) \cdot \operatorname{rect}(\delta_s, \delta_t; w_s, w_t)\, d\delta_t\, d\delta_s \,.
\end{aligned}
$$

Back

Infinitesimal vs finite-sized sensor pixel: point object

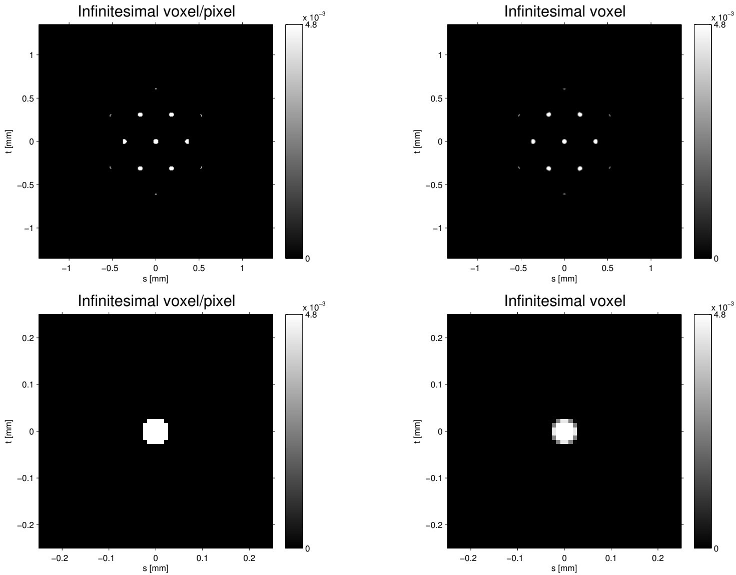

(For an infinitesimal voxel)

Infinitesimal vs finite-sized sensor pixel: sphere object

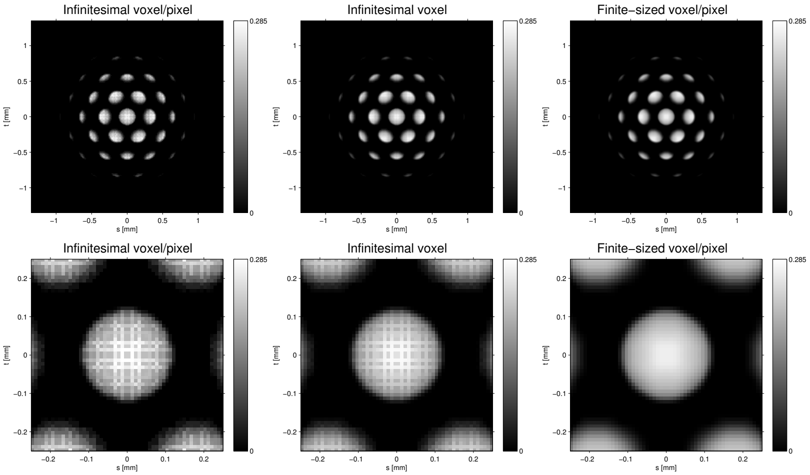

point voxel
point sensor

point voxel
finite sensor

finite voxel
finite sensor